Research Article

Construction and Verification of a Novel Pyroptosis-Related lncRNA Signature Associated with Immune Landscape in Gliomas

Xiaoqiang Feng [ID],[1,2] **Yuehua Chen** [ID],[2] **Xuanyu Liu** [ID],[2] **Zhihui Zhong** [ID],[2] and **Yanjun Liu** [ID][1]

[1]*Department of Immunology, School of Basic Medical Sciences, Southern Medical University, National Demonstration Center for Experimental Education of Basic Medical Sciences of China, Guangdong Provincial Key Laboratory of Proteomic, Guangzhou, 510515 Guangdong, China*
[2]*Center of Stem Cell and Regenerative Medicine, Gaozhou People's Hospital, Gaozhou, 525200 Guangdong, China*

Correspondence should be addressed to Yanjun Liu; yanjun@smu.edu.cn

Gliomas are the most common tumor in the central nervous system with limited prognostic markers making it difficult to research progression. Induction of cellular immunogenic death is a promising treatment for glioma. Pyroptosis is one of the recently discovered programmed immuogenic cell death modes which remains unclear in glioma. We obtained glioma datasets from the CGGA and TCGA websites. Pearson correlation analysis was used to find pyroptosis-related lncRNAs. Subsequently, the univariate, LASSO, and multivariate Cox regression were applied to construct a prognostic signature based on pyroptosis-related lncRNAs. Kaplan-Meier plots, ROC curves, and PCA were utilized for testing the prognostic performance of the signature. We conducted the univariate and multivariate Cox regressions to ascertain if the signature worked as an independent factor for predicting overall survival (OS) for individuals with glioma from other characteristics. For evaluating the immune landscape differences between the subgroups, ESTIMATE, CIBERTSORT, and ssGSEA were adopted. Additionally, biological functions and pathways of DEGs were identified by KEGG and GO. We also screened potential drugs and measured sensitivies of chemotherapeutics between the subgroups by CellMiner and pRRophetic package. Finally, shRNA was conducted to knockdown of COX10-AS1 in U87 cells to determine its relationship with pyroptosis. We successfully created an effective pyroptosis-related lncRNA signature that divided individuals into groups of low- and high-risk, and individuals in the high-risk group were with poor prognosis in comparison to the individuals in the other group. A nomogram including clinical factors and risk scores to predict the OS was built. Furthermore, the two groups appeared to have different immune landscapes; the high-risk group showed greater levels of ESTIMATE scores, immune cell infiltration, and immune checkpoints. Additionally, immune-related pathways and functions were shown to be enriched according to KEGG and GO findings. Knockdown of COX10-AS1 inhibited U87 cell growth, upregulated CASP1 and NLRP3, and released more IL1-β and IL-18 than the negative control. In summary, our study developed an lncRNA signature related to pyroptosis for OS prediction of gliomas and demonstrated its relationship with immune infiltration and drug sensitivity.

1. Introduction

It is estimated that there are 5-6 gliomas per 100,000 Americans, high invasiveness and recurrence rate of glioma result in less than a 35% 5-year overall survival (OS) rate [1, 2]. Though researchers had found that isocitrate dehydrogenase-1 (IDH1) mutation, codeletion of the short arm of chromosome 1 and the long arm of chromosome 19 (1p/19q), and O-6-Methylguanine-DNA Methyltransferase (MGMT) promoter methylation were identified as prognostic markers and therapeutic targets involved in tumor classification and progression in recent years, despite this, the OS rate does not appear to have improved significantly [3–5]. Thus, it is urgent to find more effective prognostic

factors for determining patient subgroups and providing personalized treatment guidance.

Pyroptosis, a kind of programmed cell death, differs from apoptosis, ferroptosis, and necroptosis in terms of its molecular mechanisms [6]. According to the mechanism of the activation, it can be separated into two pathways: caspase-1-dependent and caspase-1-independent. In both pathways, gasdermin D (GSDMD) is cleaved by active caspase-1 (CASP-1) to produce a free N-terminal peptide that eventually ruptures cells to release cytoplasmic components, mature IL-1β, and IL-18 [6, 7]. Previous studies mainly focused on inflammatory diseases, but mounting evidence revealed that pyroptosis played an ambiguous role in tumor progression for it may be a tumorigenic or anticancer factor [8, 9]. Ma et al. revealed that the AIM2 inflammasome, as a key signal transducer of pyroptosis, was decreased in hepatocellular carcinoma and promoted cancer progression via activation of mTOR-S6K1 pathway indicating that pyroptosis may play an anticancer role [10]. However, according to Gao et al. [11] in non-small-cell lung cancer, higher GSDMD expression was linked to worse OS, and knockdown of GSDMD inhibited tumor cell proliferation through the promotion of apoptosis and inhibition of EGFR/Akt signaling. Long noncoding RNAs (lncRNAs) are those with a size of >200 nucleotides that does not have a protein-coding function or it is low; they could serve as prognostic markers and therapeutic targets in gliomas [12]. However, rare evidence in lncRNAs correlated to pyroptosis in gliomas was found to attract our attention.

In this study, we applied bioinformatic analysis to define pyroptosis-related lncRNAs and created a prognostic signature for the prediction of OS in gliomas. Moreover, we explored potential functional pathways and drugs involved in the high- and low-risk. Our study would offer fresh perspectives on glioma diagnosis along with its tailored treatment.

2. Methods and Materials

2.1. Collection of Data. In our study, we obtained public data on RNA-seq and clinical data from the Chinese Glioma Genome Atlas (CGGA) (http://www.cgga.org.cn/) and The Cancer Genome Atlas (TCGA) (https://portal.gdc.cancer.gov/). CGGA data (mRNAseq_693 and mRNAseq_325) were merged by the function of 'ComBat' in the 'SVA' R package and selected as the training cohort in our study, in the same way, TCGA-LGG and TCGA-GBM were merged and selected as the validated cohort. We chose 156 pyroptosis-related protein-coding genes from the Genecard dataset (https://www.genecards.org/) via the keyword of "pyroptosis" and listed in Supplementary Table 1.

2.2. Developing Pyroptosis-Related lncRNA Signature. Firstly, pyroptosis-related lncRNAs were found with the Pearson correlation analysis, lncRNAs with the absolute value of correlation coefficient > 0.3 and $p < 0.001$ were selected for further analysis, and the lncRNA-mRNA network was visualized by Cytoscape software. Univariate Cox regression was carried out to search prognostic pyroptosis-related

lncRNAs by a cut-off of $p < 0.001$. We then employed the least absolute shrinkage and selection operator (LASSO) Cox regression to reduce overfitting genes. Finally, we employed the multivariate Cox regression for establishing a pyroptosis-related lncRNA signature for clinical outcome prediction of individuals with glioma. Each individual's risk score was determined:

$$
\begin{aligned}
\text{Risk score} = &(0.2499 * \text{UBA6} - \text{AS1 expression}) \\
&+ (0.1932 * \text{COX10} - \text{AS1 expression}) \\
&+ (0.1877 * \text{LINC00092 expression}) \\
&+ (0.1865 * \text{KDM1A} - \text{AS1 expression}) \\
&+ (0.126 * \text{LINC00665 expression}) \\
&+ (0.1247 * \text{CRNDE expression}) \\
&+ (0.114 * \text{HOTAIRM expression}) \\
&+ (-0.3301 * \text{INHBA} - \text{AS1 expresion}) \\
&+ (-0.2832 * \text{TMEM254} - \text{AS1 expression}) \\
&+ (-0.2324 * \text{LINC00663 expression}) \\
&+ (-0.1981 * \text{MIR497HG expression}) \\
&+ (-0.1417 * \text{SNAI} - \text{AS1 expression}) \\
&+ (-0.1415 * \text{CHL1} - \text{AS1 expression}) \\
&+ (-0.131 * \text{GDNF} - \text{AS1 expression}) \\
&+ (-0.0655 * \text{LINC01088 expression}).
\end{aligned}
$$

$$(1)$$

Patients were sorted into high- and low-risk as per their median value. Then, we estimated the survival rates of the two risk groups using the Log-rank test and the Kaplan-Meier survival curves. Through the use of the R packages "survival," "survminer," and "timeROC," the receiver operating characteristic (ROC) curve analysis was performed to evaluate the prediction power of the signature. Principal Component Analysis (PCA) was created by the 'prcomp' function of the 'ggplot' package. Furthermore, we created a nomogram integrating risk score and significant clinical factors (age, chemotherapy status, radiotherapy status, and grade) by the 'rms' R package. The formula was also used to validate the efficacy of the TCGA cohort.

2.3. Immune Cell Infiltration Analysis of the Signature. We performed the ESTIMATE algorithm for calculating immune and stromal scores of glioma patients [13], and CIBERSORT helped in observing the proportion of 22 types of immune cells infiltrated in the tumor microenvironment [14]; furthermore, single sample gene set enrichment analysis (ssGSEA) was carried out to assess immune function status in the two groups by GSVA 1.36.3 [15].

2.4. GO and KEGG Analysis of DEGs. For exploring the potential functional annotation and pathways in the risk groups, we employed the 'limma' R package to find differentially expressed genes (DEGs, |logFC| > 1 and $p < 0.05$), while the low-risk group was the control. The 'clusterProfiler' R package was utilized to visualize Kyoto Encyclopedia
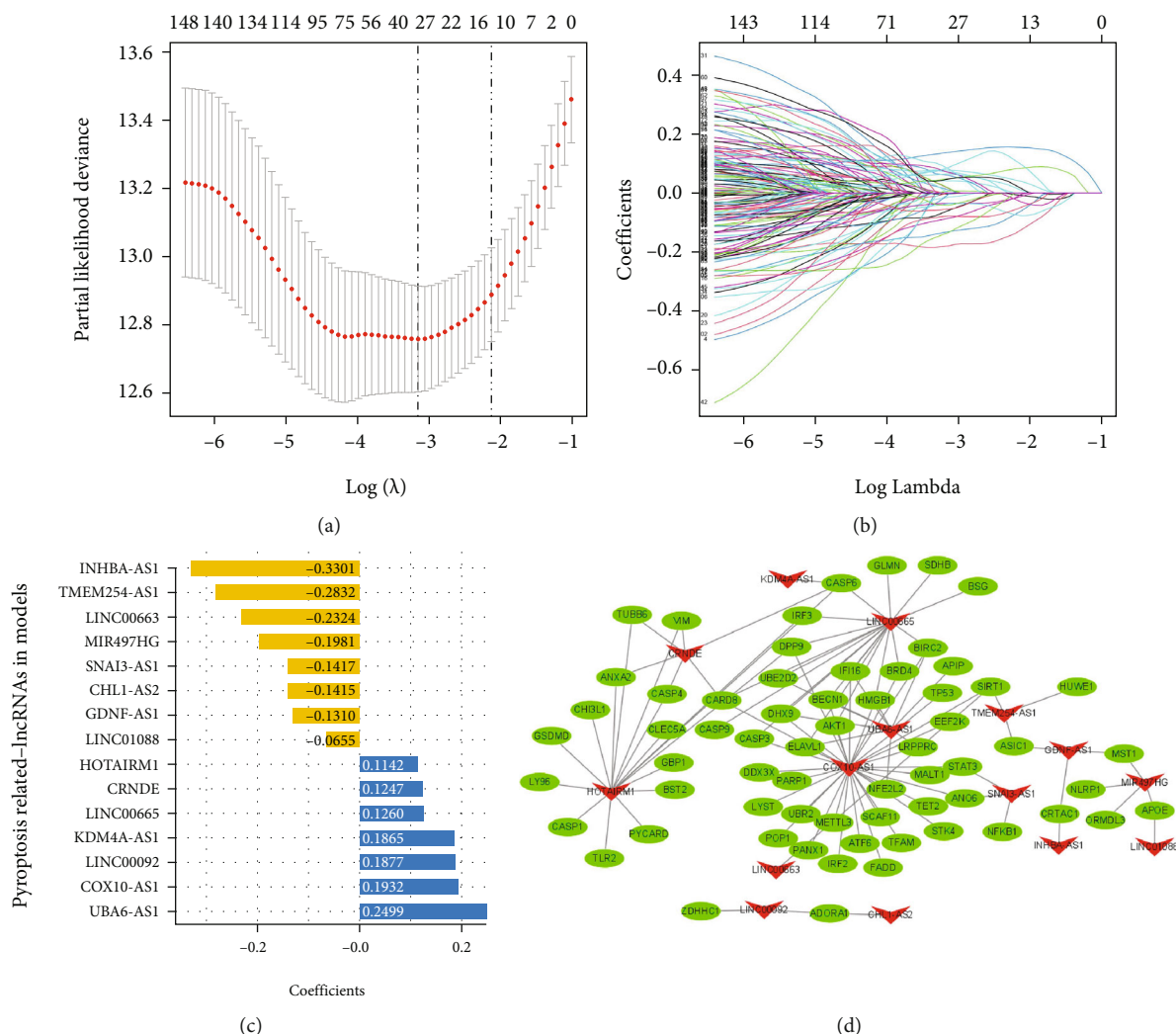
Figure 1: Identification and construction of a pyroptosis-related lncRNAmodel in the CGGA cohort. (a, b) LASSO Cox regression analysis for reducing overfitting risk pyroptosis-related lncRNAs. (c) The bar plot shows the coefficient values of signature risk lncRNAs analyzed by the multiCox analysis. (d) mRNA-lncRNA network visualized by the Cytoscape.

of Genes and Genomes (KEGG) pathways and Gene Ontology (GO) functional annotation.

2.5. The Analysis of Risk Scores and Tumor Mutation Burden (TMB).
Firstly, we analyzed the correlation of TMB scores and risk scores by the Spearman method, and the 'limma' R package was used to determine the difference of TMB between the high- and low-risk groups. The data of gene variation in glioma was also downloaded from the TCGA website. And the top 20 genes with the highest mutation rates were displayed.

2.6. Drug Sensitivities and IC50 Evaluation.
The CellMiner database is a relational database tool to store, query, and integrate as well as retrieve molecular profile data on the NCI-60 along with other cancerous cells [16, 17]; we included the drugs under clinical trial or FDA approved, while correlation value $|cor| > 0.3$ and $p < 0.01$ were preserved to find potential drugs associated with the expression of risk lncRNAs (Supplementary Table 3). And the

'pRRophetic' package was applied to predict the IC50 values of specific compounds from the Genomic of Drug Sensitivity in Cancer (GDSC).

2.7. Cell Culture and Transfection.
We purchased normal microglial cell line HMC3 and glioma cell line U87 from BeiNa Culture Collection Company; then, cell lines were cultured with DMEM medium (Gibco Company) that contained 10% fetal bovine serum (FBS, Gibco Company) at 37°C and 5% CO_2. sh-COX10-AS1 and sh-NC were synthesized by Genpharma (Shanghai, China). We transfected the plasmid of sh-COX10-AS1: 5′-GCTGGCAAAGAGAAAG CTTGT-3′ and sh-NC: GTTCTCCGAACGTGTCACGT into the U87 cell line by Lipofectamine 2000 (Invitrogen) for 48 hours based on specific protocols.

2.8. Extraction of RNA and Quantitative Real-Time PCR.
To extract the total RNA, a kit of EZBioscience (Roseville, US) was employed; then, we measured RNA concentration and purity by Nanodrop (Thermofisher) and was reversed to

CGGA cohort
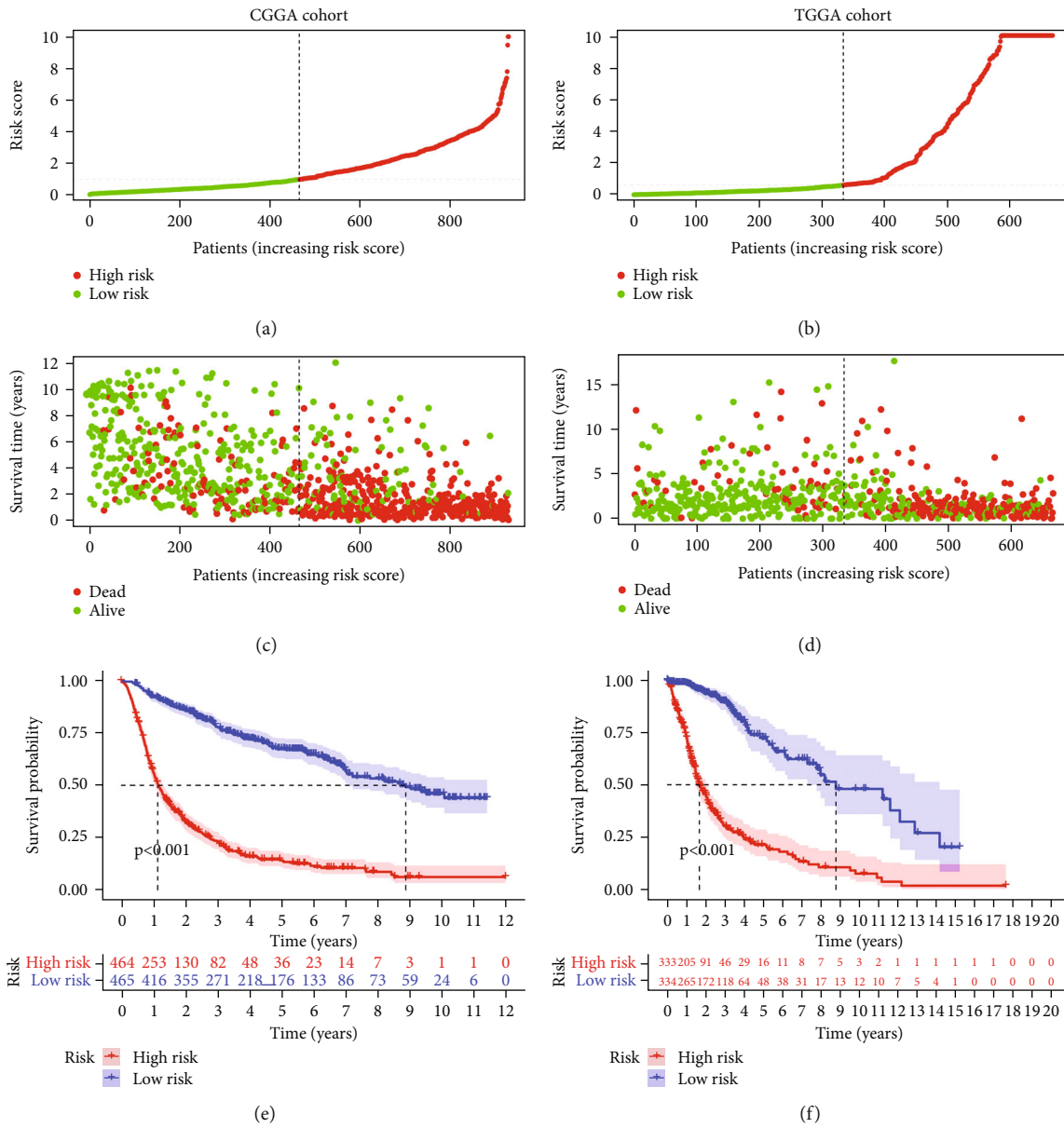
(a)

TGGA cohort

(b)

(c)
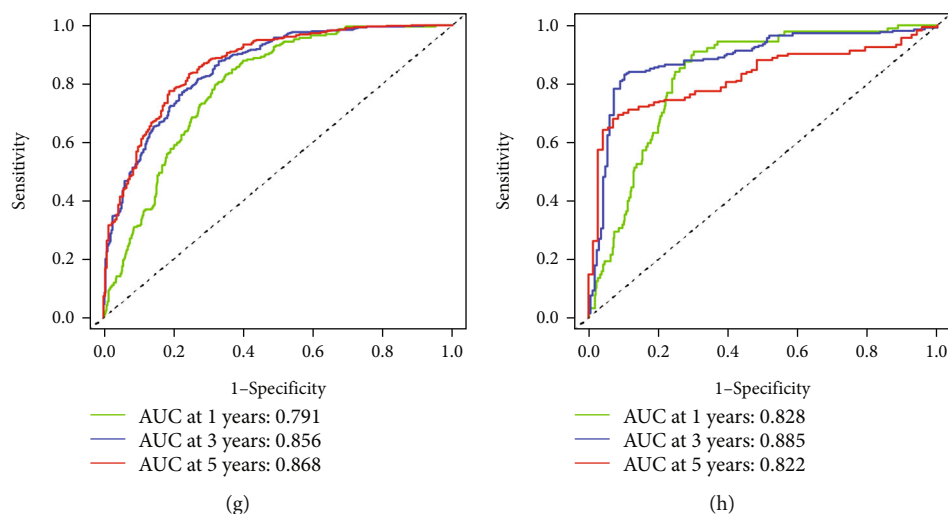
(d)

(e)

(f)

FIGURE 2: Continued.

FIGURE 2: Construction of a pyroptosis-related lncRNAs signature in the CGGA cohort and validation by the TCGA cohort. (a, e) Divided individuals into high- and low-risk groups as per median risk score. (b, f) Distribution of survival status in the high- and low-risk groups. (c, g) K-M plot displayed the survival difference between the high- and low-risk groups. (d, h) ROC curves for assessing predicting power of constructed prognostic signature.

complementary DNA (cDNA) by HiScript III-RT SuperMix for qPCR (+gDNA wiper) (Vazyme, Nanjing, China). Subsequently, we conducted qPCR by ChamQ Universal SYBR qPCR (Vazyme, Nanjing, China) and detected by 7500 Real-Time PCR System (Thermofisher, US); the relevant gene expression was calculated via $2^{-\Delta\Delta CT}$. COX10-AS1 and GAPDH primers were synthesized by Sangon Biotech. The COX10-AS1 sequence: $5'$-TATCGAACGGTACTTG CTTACG-$3'$ (F), $5'$-TGGCTAGTGACCCGGTAGTCA-$3'$ (R); CASP1 sequence: $5'$-TTTCCGCAAGGTTCGATTT TCA-$3'$ (F), $5'$-GGCATCTGCGCTCTACCATC-$3'$ (R); NLRP3 sequence: $5'$-GATCTTCGCTGCGATCAACAG-$3'$ (F), $5'$-CGTGCATTATCTGAACCCCAC-$3'$ (R); GAPDH sequence: $5'$-GAAGGTGAAGGTCGGAGTC-$3'$ (F), $5'$-GAAGATGGTGATGGGATT TC-$3'$ (R).

2.9. Cell Counting Kit-8 (CCK-8) Assay.
Using the CCK-8 assay (GLPBIO, Montclair, CA, USA), cell proliferation after transfection was quantified. Cells were grown in 96-well plates at 1000 per well with DMEM medium and 10% FBS. $10\,\mu$l CCK-8 solution was transferred to each well at the appointed time for incubation at 2 h; then, we detected the 450 nm absorbance values via microplate spectrophotometer (Thermofisher, USA) to determine the ability of transfected cell proliferation.

2.10. Enzyme-Linked Immunosorbent Assay (ELISA).
We collected cell supernatant for measuring IL-1β and IL-18 by ELISA kit (Boster, Wuhan, China) following the procedure of introduction. Briefly, coated plates were added by the supernatant from transfected cells and detected by ELISA detection antibodies.

2.11. Statistical Analysis.
R software (4.1.1) and GraphPad Prism (8.0) were utilized for statistical analyses. Kaplan-Meier analysis was employed for the assessment of OS differ- ences in both risk groups. Wilcoxon test was employed for comparing the variation of immune cells, and the level of checkpoint expression in the two groups. Cox regression analyses, both univariate and multivariate, were used to examine independent clinical variables. Student's t-test or one-way ANOVA test was employed for comparing immune scores, stromal scores, ESTIMATE scores, and the expression levels of CASP1, NLRP3, IL-1β, and IL-18. Data were reported as mean $\pm$ SEM. $p < 0.05$ was taken as a significant value.

3. Results

3.1. Identifying the Pyroptosis-Related Prognostic lncRNAs.
We obtained an expression matrix of 156 genes linked with pyroptosis from CGGA datasets; the Pearson correlation analysis was applied for screening pyroptosis-related lncRNA ($|Cor| > 0.3$, $p < 0.001$), and 743 lncRNAs linked with pyroptosis were found in our study. To uncover those prognostic pyroptosis-related lncRNAs in gliomas, we used the univariate Cox regression to search the 743 lncRNAs and found 165 prognostic pyroptosis-related lncRNAs. Then, we applied the LASSO Cox regression for reducing the overfitting risk of the 165 lncRNAs, and 28 lncRNAs were screened out (Figures 1(a) and 1(b)). Finally, we measured the coefficient values by the multivariate Cox analysis for establishing a prognostic pyroptosis-related lncRNAs model, and fifteen lncRNAs were left, including eight favorable prognostic factors (INHBA-AS1, TMEM254-AS1, LINC00663, MIR497HG, SNAI3-AS1, CHL1-AS2, GDNF-AS1, and LINC01088, HR < 0, $p < 0.001$) and seven poor prognostic factors (HOTAIRM1, CRNDE, LINC00665, KDM4A-AS1, LINC00092, COX10-AS1, and UBA6-AS1, HR > 0, $p < 0.001$) (Figure 1(c)). The interaction network of reserved fifteen lncRNA with mRNA is shown in Figure 1(d).
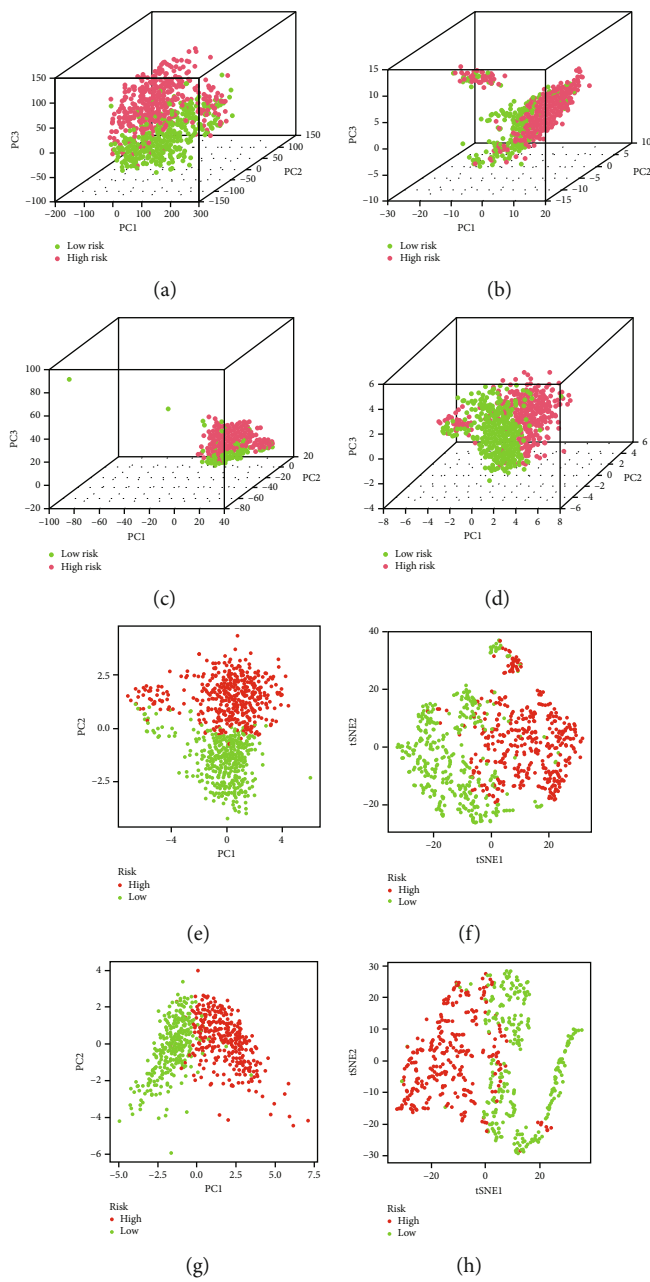
(a)

(b)

(c)

(d)

(e)

(f)

(g)

(h)

Figure 3: Continued.
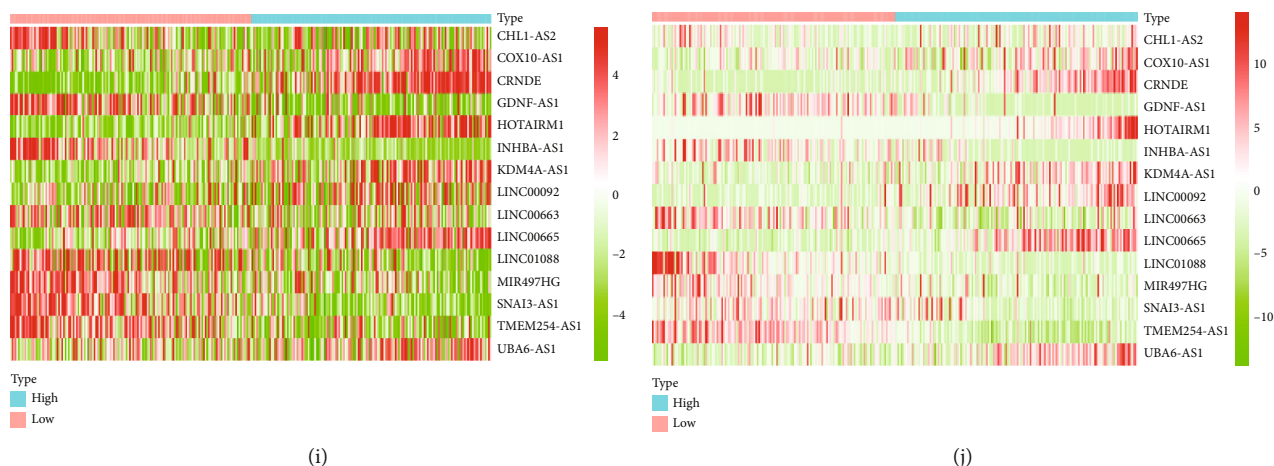
(i)   (j)

FIGURE 3: Separation of the high- and low-risk glioma patients by PCA and *t*-SNE analysis. (a–d) 3D-PCA plot for the whole genome (a) pyroptosis-related genes, (b) all pyroptosis-related lncRNAs (c) and signature pyroptosis-related lncRNAs, (d) separation of the high- and low-risk groups in the CGGA cohort. (e–h) 2D-PCA and *t*-SNE plot for signature pyroptosis-related lncRNAs separation of the high- and low-risk groups in the CGGA cohort (e, f) and the TCGA cohort (g, h). (i, j) Expression levels of signature lncRNAs in the high- and low-risk groups in the CGGA cohort (i) and the TCGA cohort (j).

3.2. Development and Validation of Pyroptosis-Related lncRNA Prognostic Model.

As per the result of the multivariate Cox, we created a prognostic signature of pyroptosis-related lncRNAs in the CGGA cohort. Each individual's risk score was measured with the formula mentioned in the Materials and Methods and individuals were separated into high-risk ($n = 464$) and low-risk ($n = 465$) groups by the median value of risk scores 1.0161 (Figure 2(a)). The distribution plot showed the association between risk scores and survival status that higher scores indicated more deaths in gliomas; on the other hand, more patients at alive status with lower risk scores suggested that patients in the low-risk group were with longer survival time (Figure 2(b)). Additionally, the Kaplan-Meier curves indicated that those in the high-risk group had lower survival times in comparison to individuals in the low-risk group (Figure 2(c), $p < 0.001$). ROC analysis was employed to assess the prediction power of our prognostic signature, and the respective AUCs of 1-, 3-, and 5-year OS were 0.791, 0.856, and 0.868, respectively, (Figure 2(d)).

Meanwhile, the TCGA dataset as a validated cohort was included in our study to test the performance of our prognostic signature. The outcomes of the validated cohort were in accord with those in the CGGA cohort, individuals with higher risk scores had worse survival outcomes in comparison to individuals with lower risk scores (Figures 2(e)–2(g)), and high accuracy of AUC for 1-, 3-, and 5-year OS was found (Figure 2(h), 0.828, 0.885, and 0.822, respectively). Additionally, we performed 3D- and 2D-PCA and *t*-SNE to analyze the difference in distribution patterns between the two subgroups. 3D-PCA plots showed that the whole genome, pyroptosis-related genes, all pyroptosis-related lncRNAs that without analyzing by the Cox regression could not effectively separate patients with glioma into two groups in the CGGA cohort (Figures 3(a)–3(c)), but our model based on the prognostic lncRNAs defined by the LASSO Cox regression had accurate performance and helped in

dividing the individuals into high- and low-risk groups (Figure 3(d)); we also confirmed that the model had a potential to distinguish patients into discrete directions by using 2D-PCA and *t*-SNE plots (Figures 3(e)–3(h)). Furthermore, the relationship between risk scores and expression level of risk genes in our signature is shown in Figures 3(i) and 3(j). We found that favorable prognostic factors (INHBA-AS1, TMEM254-AS1, LINC00663, MIR497HG, SNAI3-AS1, CHL1-AS2, GDNF-AS1, and LINC01088) were increased with risk scores, but the other genes had a reverse tendency. These results suggest that our newly created prognostic pyroptosis-related lncRNA signature might reliably predict the survival of patients with glioma with good accuracy.

3.3. Validation of the Clinical Independence of Pyroptosis-Related lncRNA Prognostic Model and Construction of a Predictive Nomogram.

In our investigation, the univariate and multivariate Cox regression analyses were used to see if the signature was an independent predictor of glioma patients' OS, separate from other clinical variables. The outcomes of the univariate Cox regression revealed that the risk score was a significant independent factor linked to OS (CGGA cohort: HR = 1.466, 95% CI = 1.409-1.525, $p <$ 0.001; TCGA cohort: HR = 1.329, 95% CI = 1.065-1.625, p < 0.001) (Figures 4(a) and 4(b)), and the findings of the multivariate Cox regression analysis still supported this finding (CGGA cohort: HR = 1.313, 95% CI = 1.246-1.383; TCGA cohort: HR = 2.354, 95% CI = 2.062-2.628) (Figures 4(c) and 4(d)).

As per the findings of the multivariate Cox regression analysis in the CGGA cohort, we created a nomogram integrating the risk score and clinical factors of age, chemotherapy, radiotherapy, status, and grade for comprehensively predicting the glioma patients' OS at 1, 3, and 5 years, and its concordance index (*C*-index) of our nomogram was 0.77 (Figure 5(a)). The calibration curves showed that the

	pvalue	Hazard ratio
Grade	<0.001	2.865(2.521–3.257)
Gender	0.952	1.006(0.840–1.204)
Age	<0.001	1.028(1.020–1.036)
Radio.stat	0.672	0.948(0.741–1.213)
Chem.stat	<0.001	1.588(1.290–1.956)
IDH.stat	<0.001	0.319(0.265–0.383)
riskScore	<0.001	1.466(1.409–1.525)

Hazard ratio

(a)

	pvalue	Hazard ratio
Age	<0.001	1.065(1.055–1.076)
Gender	0.028	1.342(1.032–1.744)
Grade	<0.001	4.660(3.814–5.693)
Chem.stat	<0.001	1.970(1.424–2.727)
Radio.stat	<0.001	1.828(1.305–2.560)
IDH.mutation	<0.001	0.204(0.096–0.433)
riskScore	<0.001	1.329(1.056–1.625)

Hazard ratio

(b)

	pvalue	Hazard ratio
Grade	<0.001	2.151(1.838–2.517)
Gender	0.915	0.990(0.826–1.187)
Age	0.006	1.010(1.003–1.018)
Radio.stat	0.002	0.668(0.516–0.864)
Chem.stat	0.035	0.782(0.622–0.983)
IDH.stat	0.292	0.882(0.699–1.114)
riskScore	<0.001	1.313(1.246–1.383)

Hazard ratio

(c)

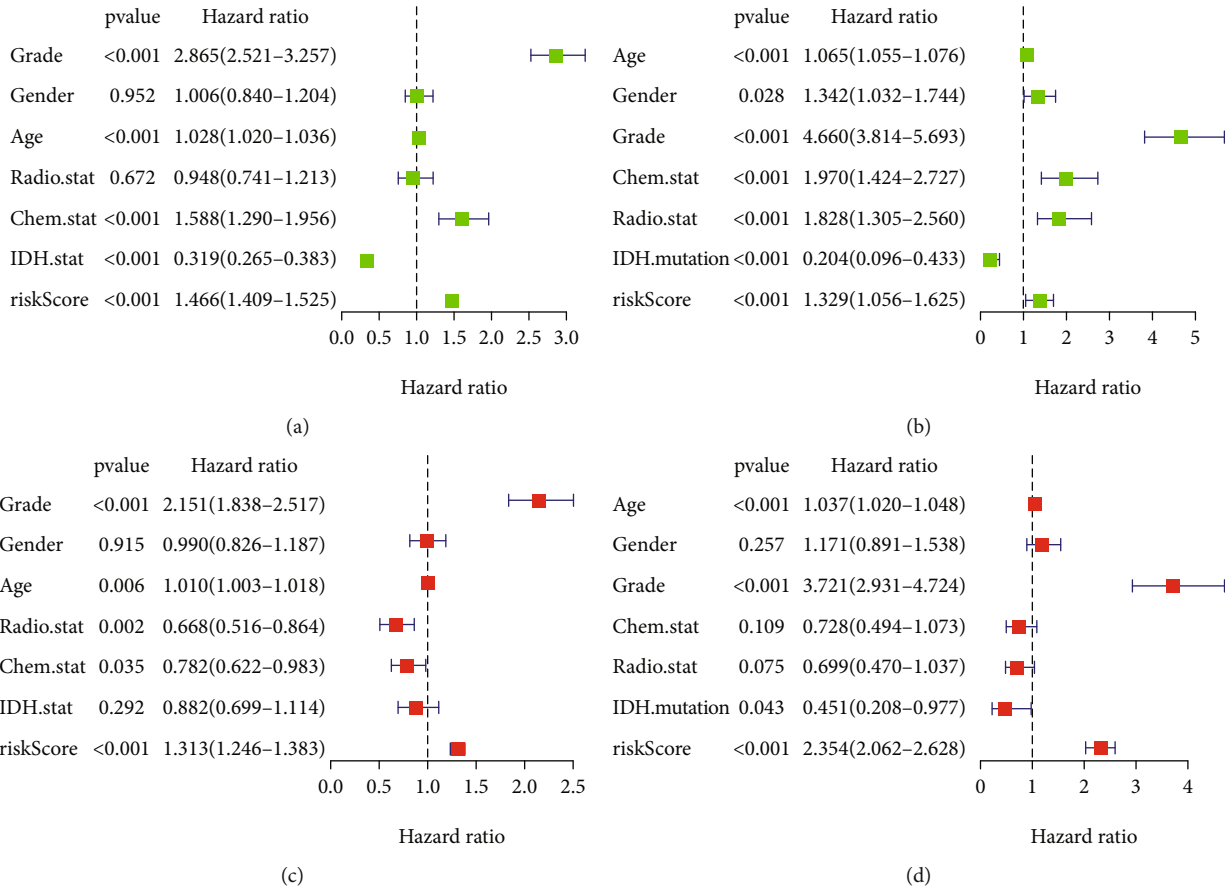|	pvalue	Hazard ratio
Age	<0.001	1.037(1.020–1.048)
Gender	0.257	1.171(0.891–1.538)
Grade	<0.001	3.721(2.931–4.724)
Chem.stat	0.109	0.728(0.494–1.073)
Radio.stat	0.075	0.699(0.470–1.037)
IDH.mutation	0.043	0.451(0.208–0.977)
riskScore	<0.001	2.354(2.062–2.628)

Hazard ratio

(d)

FIGURE 4: Univariate and multivariate Cox regression analyses of the risk scores and clinical features relating to OS in the training cohort (a, b) and the testing cohort (c, d).

predicted mortality was close to the actual mortality (Figure 5(b)). The ROC curves of 1-, 3-, and 5-year OS exhibited high accuracy (0.818, 0.860, and 0.853, respectively) (Figure 5(c)). These findings revealed that the signature was an independent factor and the nomogram can potentially be an excellent tool in applying for predicting survival outcomes of individuals with glioma.

3.4. The Difference in Immune Landscape Biological Pathways and TMB among the Two Groups. The immune microenvironment was of great importance in tumor progression, we applied the ESTIMATE, CIBERTSORT, and ssGSEA methods for exploring the difference in immune/stromal scores, immune cell infiltration, immune checkpoint, and immune functions among the two risk groups. ESTIMATE outcomes revealed that stromal and immune scores were considerably greater in the high-risk group (Figure 6(a)). We analyzed 22 kinds of immune cells in glioma by CIBERTSORT "R" package, the immune cell infiltration level differed significantly between the two subgroups. CD8+ T cells, regulatory T cells, follicular helper T cells, resting NK cells, gamma delta T cells, M0 macrophage cells, M1 macrophage cells, M2 macrophage cells, and neutrophils were observed with higher abundance in the high-risk group, while in the low-risk group, resting CD4+ memory T cells, monocytes, activated NK cells, activated dendritic

cells, resting mast cells, activated mast cells, and eosinophils were increased (Figure 6(b)). And ssGSEA method was employed to test immune functions between the two groups; the findings revealed that scores of all immune functions were greater in the high-risk group (Figure 6(c)). Immune checkpoint blockade was an important strategy for glioma treatment; several regular checkpoint molecules were included in our study, and it indicated that except for PVRIG, CD200, and VTCN1, immune checkpoints were substantially higher in the high-risk group (Figure 6(d)). These outcomes suggested that the immune microenvironment was different in the two groups, which may provide personal immunotherapy as per the risk score.

Subsequently, we identified the potential biological pathways and functions as per the differential expression genes (DEGs) among the two groups by KEGG and GO analysis. In GO analysis, immune-related biological pathways (BPs) such as neutrophil activation involved in immunity and degranulation, response to interferon-gamma, humoral immune response, cell component (CC) MHC protein complex, and molecular function (MF) antigen binding were uncovered (Figures 7(a) and 7(b)). Consistent with the GO analysis, the KEGG pathways also showed that phagosome complements the coagulation cascade of immunological pathways (Supplementary Figures S1(A) and S1(B)). Our
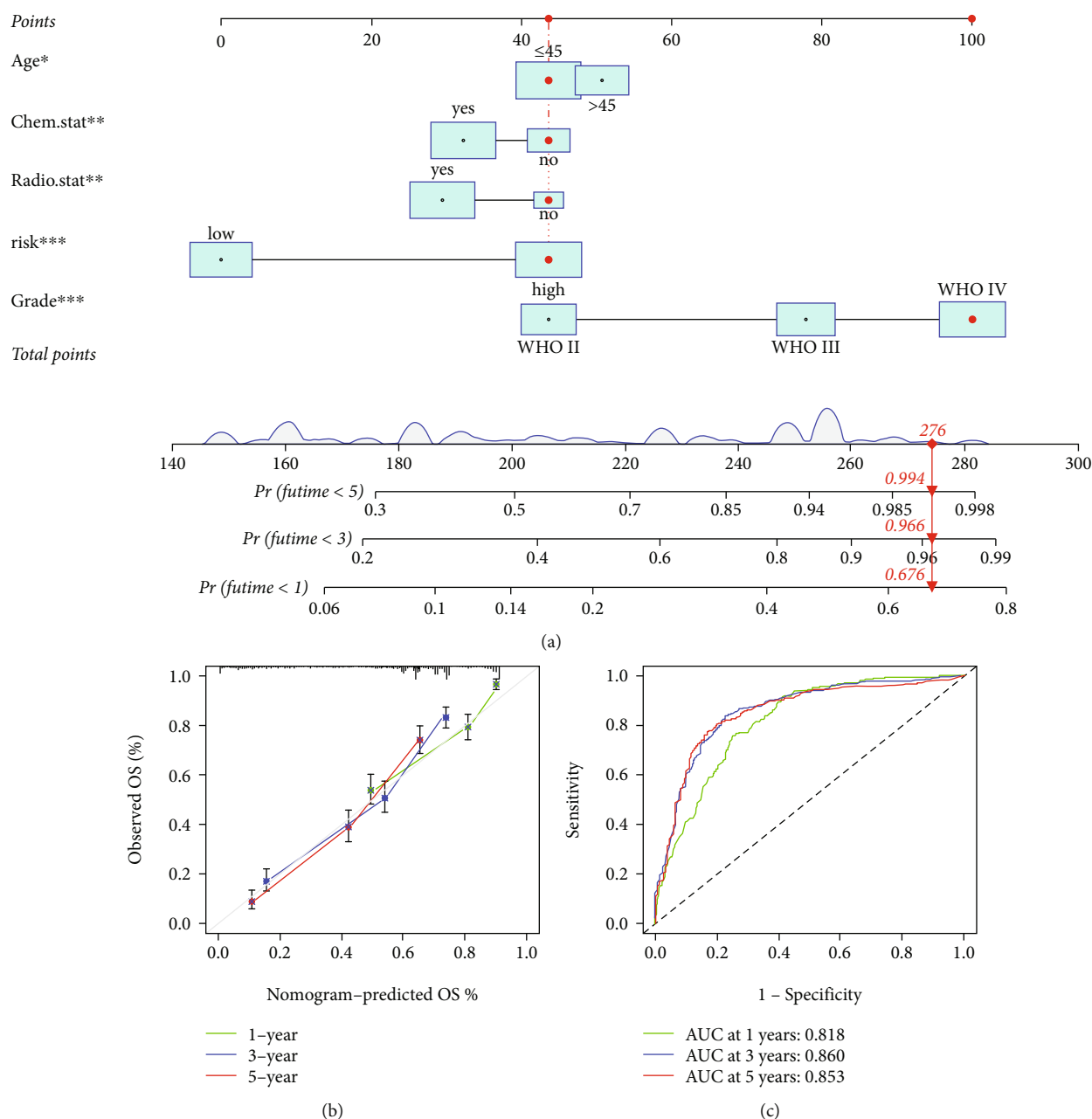
(a)

(b)

(c)

FIGURE 5: Construction of a nomogram for predicting 1-, 3-, and 5-year OS of glioma patients. (a) Nomogram including age, chemotherapy status, radiotherapy status, risk scores, and grade. (b, c) Calibration curves and ROC curves showed the 1-, 3-, and 5-year OS prediction power of nomogram. $^*p < 0.05$, $^{**}p < 0.01$, $^{***}p < 0.001$.

findings revealed that the immune-related pathways were vital in tumor progression.

Futhermore, we analyzed the correlation of TMB scores with risk scores; the result showed that the TMB scores were positively with risk scores ($R = 0.53$, $p < 0.001$, Supplementary Figure S2A), and TMB scores of the low-risk group were much lower than the patients of the high-risk group ($p < 0.001$, Supplementary Figure S2(B)). The top 20 genes with the highest mutation frequencies are exhibited in Supplementary Figures S2(C) and S2(D). Most patients carried mutations in the low- and high-risk groups (86.92% and 96.64%, respectively), and missense mutations

were the most frequent. The rate of TP53 mutation was the highest in the low-risk group (36%), followed by IDH1 (28%). Unexpectedly, in the high-risk group, the rate of IDH1 mutation was up to 91%, and TP53 ranked the second was 46%. These results suggested that the high- and low-risk groups in our risk signature show different environment of TMB.

3.5. Different Drug Sensitivities between Two Groups Based on Pyroptosis-Related lncRNAs Signature. To further verify whether the risk lncRNAs discovered by our study had the potential to be good candidates for therapy targets, we
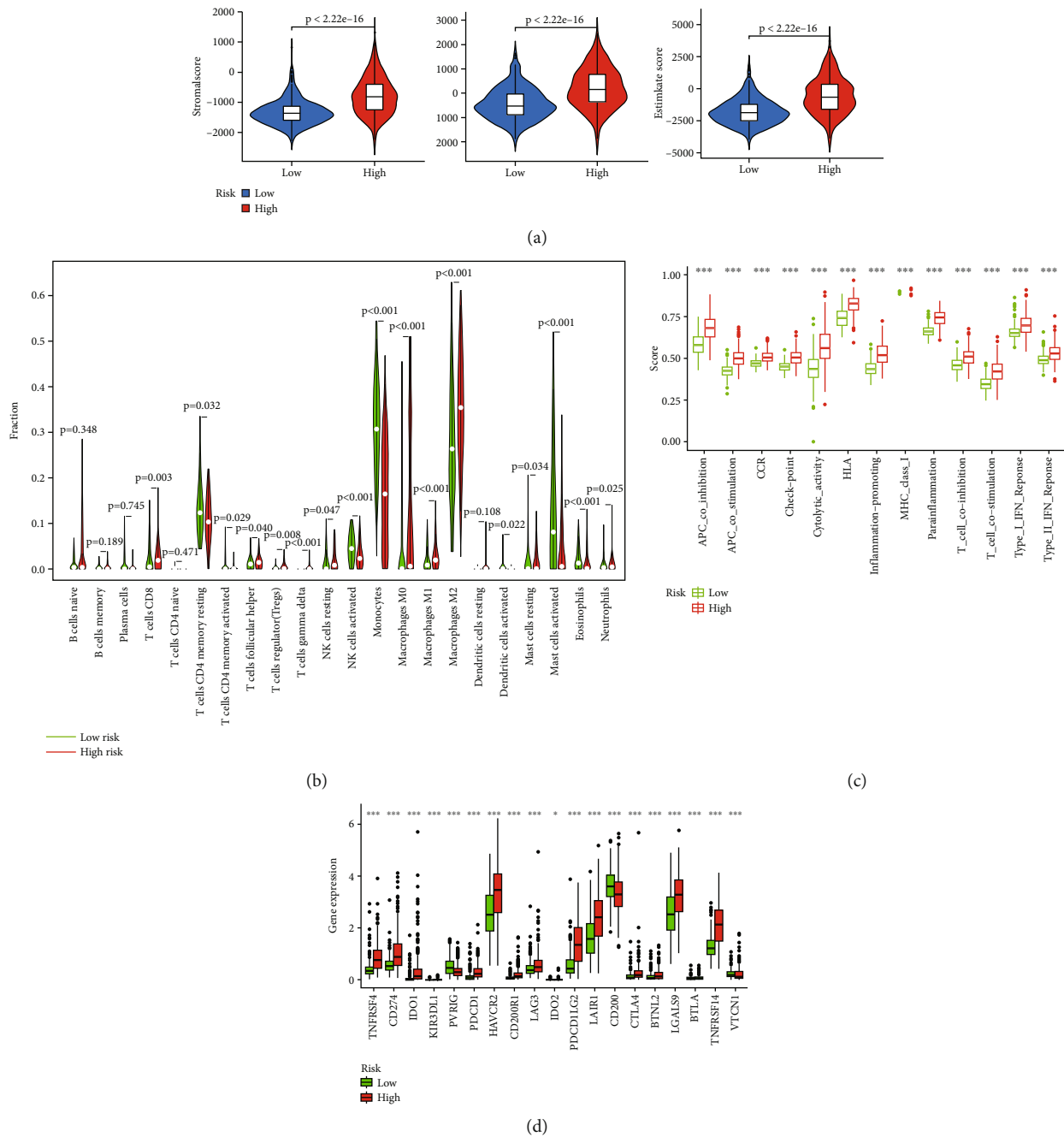
(a)

(b)

(c)

(d)

FIGURE 6: The difference in immune landscape among the high- and low-risk groups. (a) Stromal score, immune score, and ESTIMATE score difference between the high- and low-risk groups. (b) 22 types of immune cell infiltration levels in the high- and low-risk groups by CIBERTSORT. (c) Immune function difference among the high- and low-risk groups. (D) Immune checkpoint difference of the high- and low-risk groups. $^*p < 0.05$, $^{**}p < 0.01$, $^{***}p < 0.001$.

studied the drug sensitivity of 707 kinds of compounds that had been approved by the FDA or under clinical trials through the CellMiner database. We only included candidate drugs while the |Cor > 0.3| and $p < 0.01$ (Supplementary Table 3), concerning the top 16 most relevant correlations shown in Figure 8, we found that increased TMEM254-AS1 expression was associated with drug resistance of cells to fulvestrant, SR16157, and raloxifene. Similar results were obtained in the relationship between

LINC01088 expression and imexon, ABT-199, cyclophosphamide, hydroxyurea, chelerythrine, and fostamatinib. Besides, increased LINC0063 and LINC00665 expression were associated with drug sensitivity of cancer cells to AT-133387 and cobimetinib (isomer 1). We also applied the 'pRRophetic' package to compare six common anticancer drug sensitivities between the two risk groups; it revealed that except for gefitinib, the IC50 of cisplatin, cyclopamine, etoposide, sunitinib, and vinlastine were
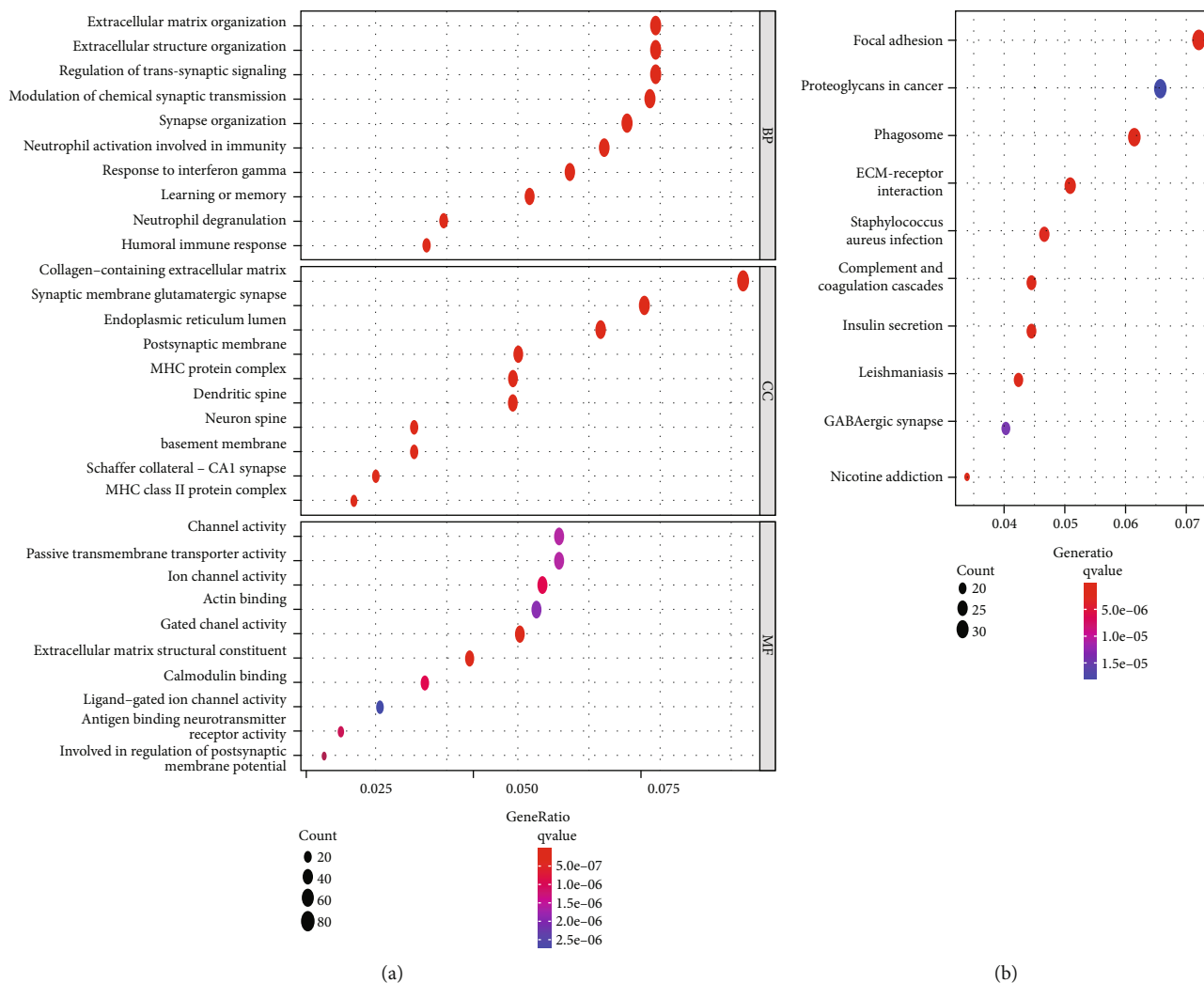
(a)

(b)

FIGURE 7: GO and KEGG pathways involved in the pyroptosis-related lncRNA signature of the CGGA cohort. (a) GO annotation. (b) KEGG pathways.

greater in the low-risk group (Figure 9). It suggested that our prognostic signature was also linked to chemotherapy treatment and may provide precise drug use for glioma patients.

3.6. Knockdown of COX10-AS1 Promoted Glioma Cell Pyroptosis. To check the association among candidate pyroptosis-related lncRNAs and pyroptosis in our signature, we chose the COX10-AS1 as the target for experiments in vitro based on the reasons that COX10-AS1 was expressed highly in glioma patients and linked with a worse prognosis [18, 19]. It was also found that it was a hub gene with the most degree in our network analyzed by cytoHubba plug-in in Cytoscape (Supplementary Table 2), but its relationship with pyroptosis in glioma cells was still unknown. Therefore, we found COX10-AS1's level of expression in normal microglial cells HMC3 and tumor cells U87 by qPCR, which revealed that the level of COX10-AS1 in tumor cells was double in comparison with

those in the HMC3 cells (1.00 ± 0.02 vs. 2.08 ± 0.1, $p < 0.05$, Figure 10(a)). Then, shRNA was applied to effectively knock down the level of COX10-AS1 expression in U87 cells (1.00 ± 0.11 vs. 0.46 ± 0.06, $p < 0.05$, Figure 10(b)). CCK-8 assay result showed that reduced expression of COX10-AS1 inhibited U87 cell proliferation (Figure 10(c), $p < 0.05$). The NLRP3 and CASP1 were the key executors in the pathway of pyroptosis [7]. We then tested the relative expression levels of CASP1 and NLRP3 by qPCR, which demonstrated that the expression levels of CASP1 (1.00 ± 0.02 vs. 3.10 ± 0.76, $p < 0.01$) and NLRP3 (1.00 ± 0.08 vs. 6.80 ± 1.7, $p < 0.05$) were increased in the group of sh-COX10-AS1 (Figures 10(d) and 10(e)). Furthermore, we found that IL-1β (50.59 ± 5.3 vs. 10.3 ± 0.56 pg/ml, $p < 0.05$) and IL-18 (117.5 ± 13.84 vs. 65.04 ± 10.55 pg/ml, $p < 0.05$) were markedly increased in sh-COX10-AS1 cells compared to the sh-NC (Figures 10(f) and 10(g)). These results suggested that downregulation of COX10-AS1 may promote pyroptosis of glioma cells.
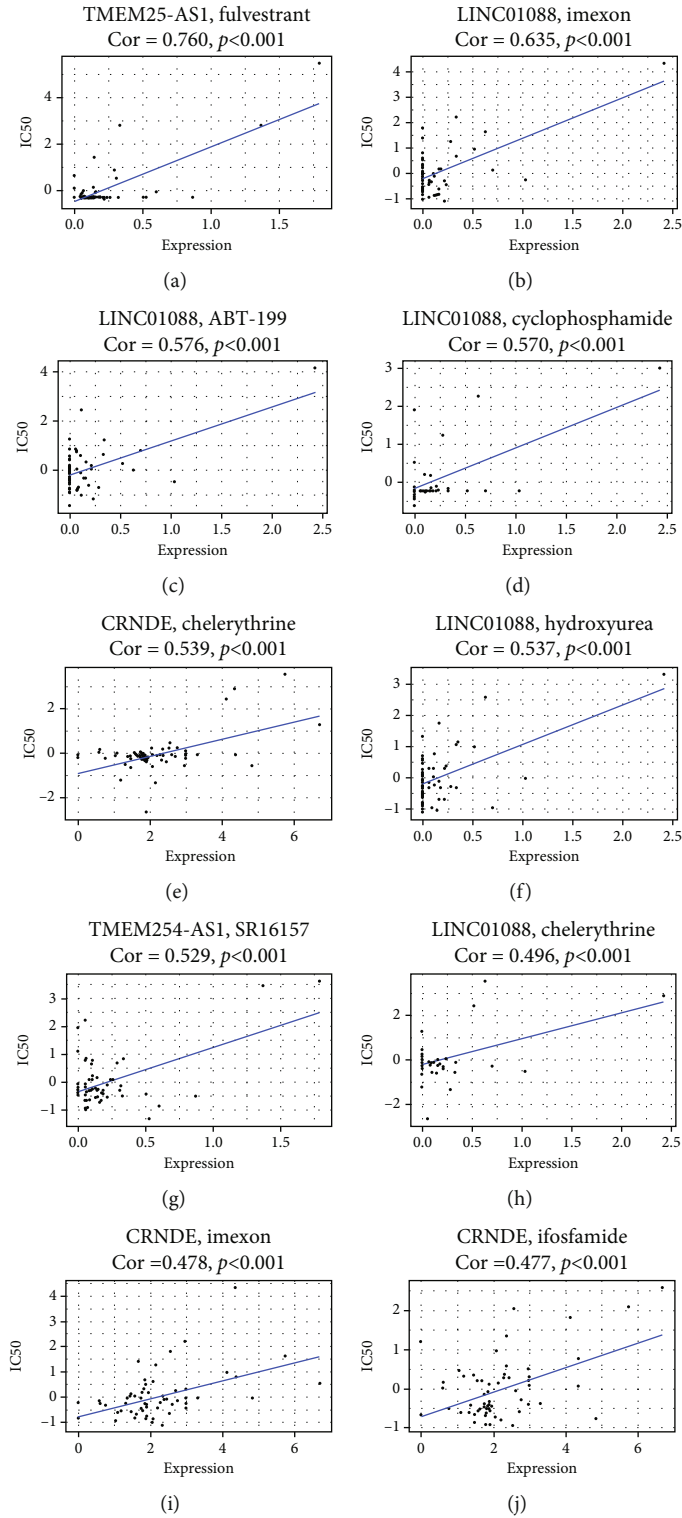
TMEM25-AS1, fulvestrant
Cor = 0.760, $p < 0.001$

(a)

LINC01088, imexon
Cor = 0.635, $p < 0.001$

(b)

LINC01088, ABT-199
Cor = 0.576, $p < 0.001$

(c)

LINC01088, cyclophosphamide
Cor = 0.570, $p < 0.001$

(d)

CRNDE, chelerythrine
Cor = 0.539, $p < 0.001$

(e)

LINC01088, hydroxyurea
Cor = 0.537, $p < 0.001$

(f)

TMEM254-AS1, SR16157
Cor = 0.529, $p < 0.001$

(g)

LINC01088, chelerythrine
Cor = 0.496, $p < 0.001$

(h)

CRNDE, imexon
Cor = 0.478, $p < 0.001$

(i)

CRNDE, ifosfamide
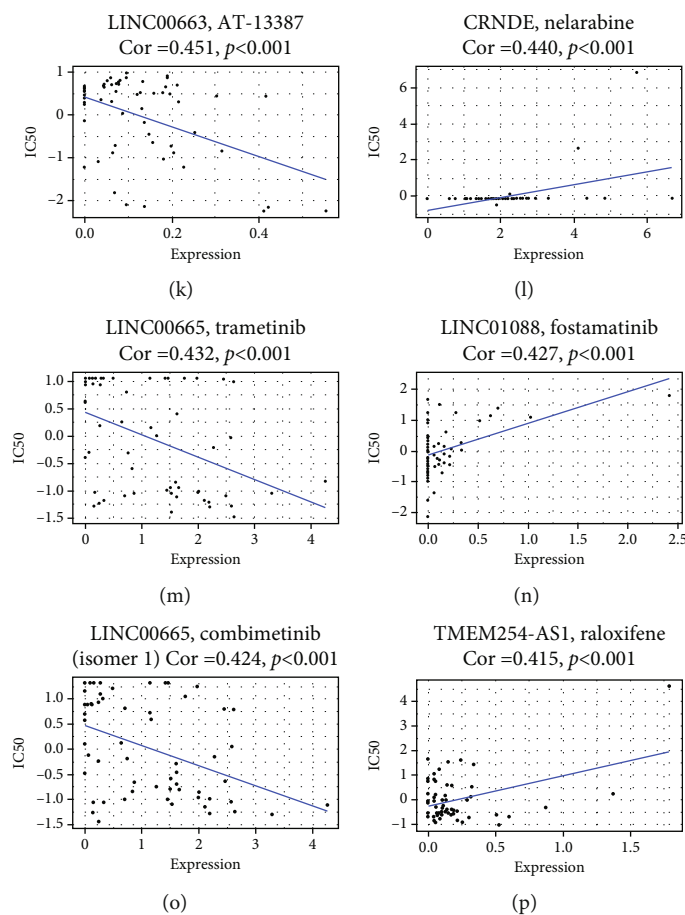Cor = 0.477, $p < 0.001$

(j)

FIGURE 8: Continued.

Figure 8: Drugs targeted signature lncRNAs and IC50 correlation analysis. (a) Fulvestrant. (b) Imexon. (c) ABT-199. (d) Cyclophosphamide. (e) Chelerythrine. (f) Hydroxyurea. (g) SR16157. (h) Chelerythrine. (i) Imexon (j) Ifosfamide. (k) AT-13387. (l) Nelarabine. (m) Trametinib. (n) Fostamatinib. (o) Cobimetinib (isomer 1). (p) Raloxifene.

4. Discussion

Gliomas such as low-grade glioma (LGG) and glioblastoma (GBM) were the most common cancer type in the brain with characteristics of insidious onset, high morbidity, and mortality that caused significant impact on health problems. Although several new molecules such as IDH1 mutation, MGMT promoter methylation, and 1p/19q chromosome codeletion have been applied for diagnosis and treatment in gliomas, the prognosis of patients remains unsatisfactory, which drives us to explore more effective and credible factors. A programmed cell death type called pyroptosis is triggered by various inflammasomes; there are two pathways: caspase-1 dependent and nondependent activation, and activated caspase cleaves gasdermins lead to the release of cell contents, as well as inflammatory factors IL-1 and IL-18 [20]. Pyroptosis in tumor plays a significantly dual role in different cancer types, it may promote cell growth, metastasis, and drug resistance; meanwhile, it also triggers an intense antitumor immune response, the pathway of pyroptosis serves as an effective potential therapeutic target in treating cancer [9, 21]. Some reports demonstrated that lncRNA is critical in the process of pyroptosis in the tumor. Ren et al. found that lncRNA ADAMTS9-AS2-stimulated

NLRP3-mediated pyroptosis through sponging miR-223-3p inhibited gastric cancer cell growth and enhanced cisplatin sensitivity [22]. In triple-negative breast cancer, cisplatin activated MEG3/NLRP3/CASP-1 pathway to induce cell pyroptosis, which suggested that MEG3 was involved in the pyroptosis pathway of cisplatin therapy [23]. Additionally, in ovarian cancer, the silencing of HOTTIP led to NLRP1 inflammasome-mediated pyroptosis by focusing on miR-148a-3p/AKT2 axis as a target [24]. These results enlighten us to find the relationship between the lncRNA, pyroptosis, and tumor progression. In our study, we successfully created an effective pyroptosis-related lncRNA signature for predicting the OS and drug sensitivities in gliomas.

We applied bioinformatics for analyzing public data sets of glioma patients from the CGGA and TCGA cohorts, for the identification of 165 prognostic lncRNAs related to pyroptosis in gliomas; we employed the Pearson correlation analysis, after ordinal analysis of the univariate, LASSO, and multivariate Cox regression; finally, fifteen pyroptosis-related lncRNAs were screened out to establish a prognostic signature. Meanwhile, Tanzhu et al. also developed a pyroptosis-related lncRNA signature for glioma patients; the ROC curves were adopted for evaluating the output of their signature, in the TCGA cohort, the respective values
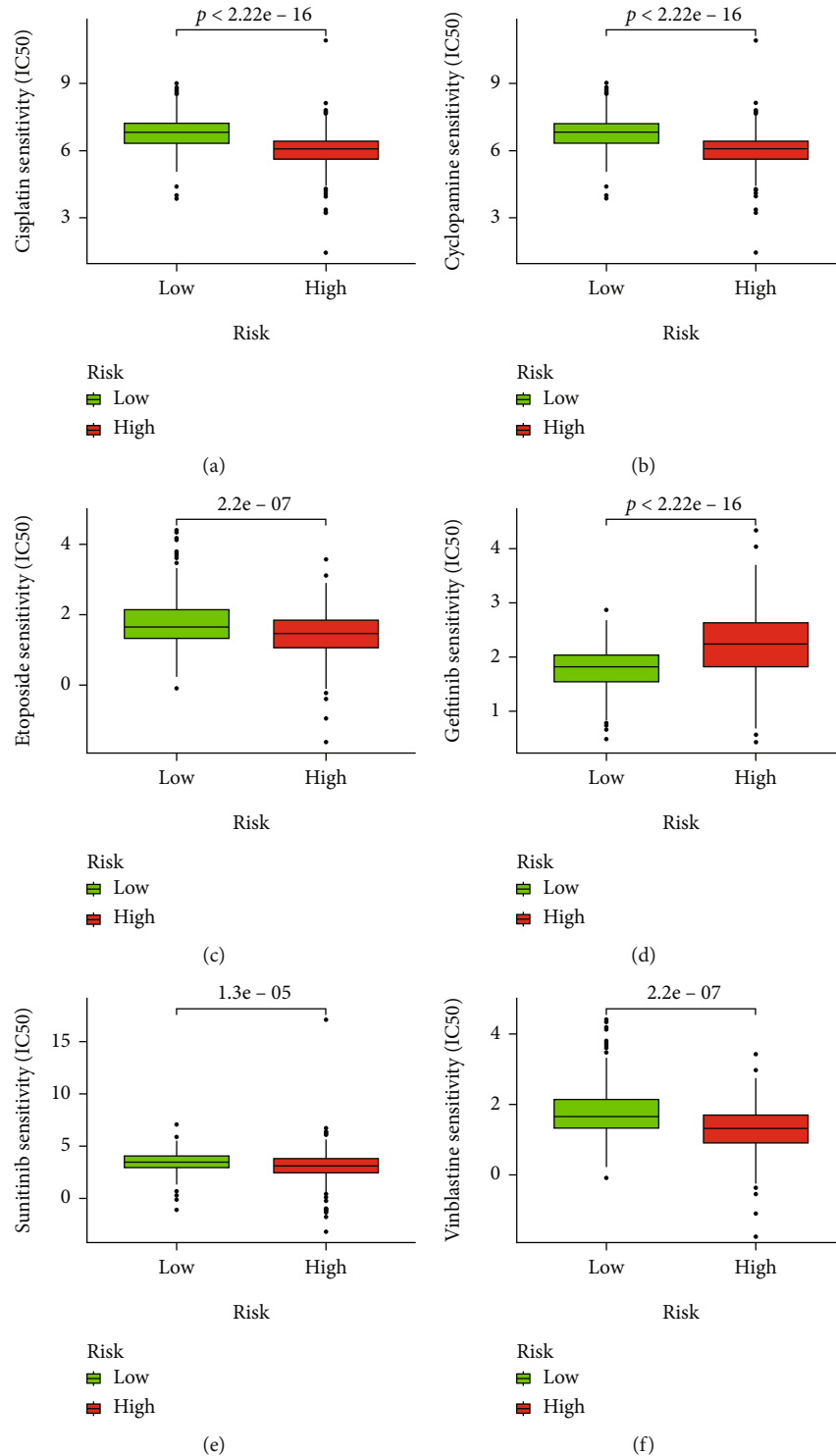
FIGURE 9: Six common chemotherapy drug sensitivity difference in the high- and low-risk groups: (a) cisplatin, (b) cyclopamine, (c) etoposide, (d) gefitinib, (e) sunitinib, and (f) vinblastine.

of 1-, 3-, and 5-year OS were 0.869, 0.886, and 0.899, respectively. It was similar to our results that are shown in Figure 2(h), but the predictive capacity of model decreased in the CGGA cohort [25]; in our signature, it still showed outstanding performance for predicting 1-, 3-, and 5-year OS. The respective AUC areas of ROC analysis were 0.791,

0.856, and 0.868, while compared to the ROC results of another published pyroptosis-related lncRNAs model in GBM patients, our signature also showed analogously excellent power of prediction [26]. It suggested that our signature was remarkable for the predictive ability validated in the CGGA and TCGA cohorts. In these studies, the analysis
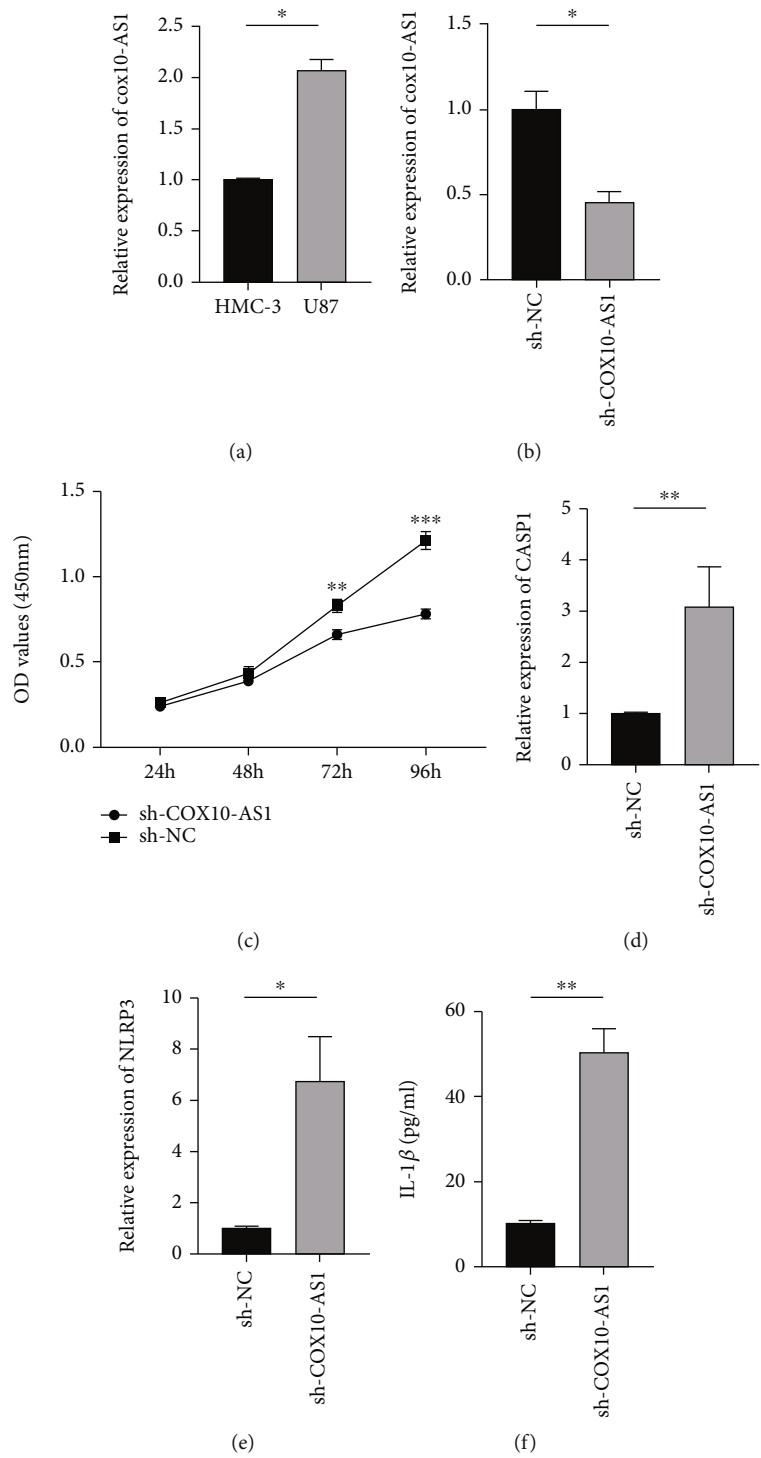
(a)

(b)

(c)
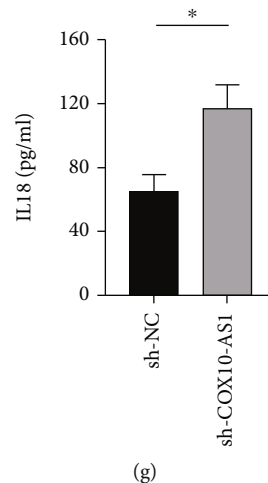
(d)

(e)

(f)

Figure 10: Continued.

(g)

FIGURE 10: Knockdown of COX10-AS1 promoted glioma cell pyroptosis. (a) Relative COX10-AS1 expression level in HMC-3 cell line and U87 cell line. (b) Knockdown of COX10-AS1 in U87 cell line by shRNA. (c) CCK-8 assays were conducted to evaluate the glioma cell proliferation in the sh-NC and sh-COX10-AS1. (d, e) Relative expressions of caspase-1 and NLRP3. (f, g) Release levels of IL-1β and IL-18. Three independent tests were done. $^*p < 0.05$, $^{**}p < 0.01$, $^{***}p < 0.001$.

methods and criteria varied from each other which may be the main reason for the different results. Moreover, for finding out that our risk signature was an independent prognostic factor, we did a univariate and multivariate analysis; afterward, a robust nomogram included risk score and clinical factors that were built as per the outcomes of the multivariate analysis, which may provide a clinical application tool for predicting OS of gliomas.

Our signature consisted of eight protective pyroptosis-related lncRNAs (INHBA-AS1, TMEM254-AS1, LINC00663, MIR497HG, SNAI3-AS1, CHL1-AS2, GDNF-AS1, and LINC01088) and seven unfavorable lncRNAs (HOTAIRM1, CRNDE, LINC00665, KDM4A-AS1, LINC00092, and COX10-AS1). Most of our risk lncRNAs had been proved to participate in tumor progression. For example, CRNDE was the most studied lncRNA of these risk genes, as an important oncogenic lncRNA that was involved in colorectal cancer [27], gastric cancer [28], and prostate cancer via various pathways [29]. In glioma, CRNDE was upregulated and promote tumor progression via attenuating miR-384/PIWIL4/STAT3 axis [30], it also contributed to temozolomide (TMZ) resistance by autophagy, knockdown of CRDNE enhanced TMZ chemosensitivity [31]. In our study, the Pearson results showed that CRNDE is closely correlated to CASP4/6/8 (cor > 0.5, data not shown), which are important executors in pyroptosis. Our study may provide new insight into CRNDE in glioma, but further experiments were needed to explore the relationship between pyroptosis and CRNDE. Zheng et al. discovered that SNAI3-AS1 and GDNF-AS1 were also acting as protective factors that are related to ferroptosis in glioma; it was consistent with our result and indicated that the two lncRNAs may simultaneously affect glioma progression via ferroptosis and pyroptosis [32]. In addition, no related studies have been found in TMEM254-AS1, CHL1-AS2, and INHBA-AS1; it may offer us innovative directions for research in glioma.

In this research, as per their median risk score values, the individuals with glioma were sorted into high- and low-risk groups, PCA and t-SNE plots confirmed that our pyroptosis-related lncRNAs could separate patients into two accurate directions, and the low-risk group's patients had an improved prognosis when compared to those in the high-risk group. To better understand the potential pathways for different survival prognoses, GO and KEGG were used to analyze DEGs between the two groups. The outcomes of GO highlighted that neutrophil activation has a role in immunity and degranulation, response to interferon-gamma, humoral immune response, MHC protein complex, MHC II class protein complex, and antigen-binding were enriched. KEGG analysis highlighted that in the immune-related pathway of the phagosome, complement and coagulation cascade, *Staphylococcus aureus* infection, Epstein-Barr virus infection, and allograft rejection were found. The results indicated that the immunological pathways that played an important role in the pyroptosis-related lncRNAs caused different OS outcomes in glioma patients. Pyroptosis-like immunogenic cell death (ICD) leads to the severe release of immunoregulatory molecules of IL-1β, IL-18, HMGB1, and ATP [33–35], and pyroptotic cancer cells were uptaken by antigen-presenting cells which suggested that pyroptosis were closely correlated to immune activity [35, 36]. Thus, it was critical to find out the link between tumor immune microenvironment and pyroptosis-related lncRNAs signature. Firstly, we employed the ESTIMATE method to find that the immune risk scores, as well as the stromal scores of the high-risk group, were higher, CIBERTSORT results showed that this group also had the most enriched immune cells, while the activated NK cells, monocytes, resting CD4+ memory T cells, activated dendritic cells, resting mast cells, activated mast cells, and eosinophils were more abundant in the low-risk group, immune function scores were all higher in the high-risk group. As per these outcomes, the pyroptosis-related

lncRNA signature was highly correlated to the immune landscape in the microenvironment of glioma. Moreover, when the difference in immune checkpoints was assessed in the two groups, it was found that the checkpoint expression was higher in the high-risk group as well. Though the high-risk group is with more immune cell infiltration and higher immune function scores, the checkpoints expressed higher meant a more intense immunosuppressive environment in the high-risk group, which potentially contributed to poorer survival of patients in the high-risk group. Hou et al. showed that PD-L1 blockaded therapy could induce cancer cell apoptosis to pyroptosis by mediating gasdermin C expression and facilitating necrosis [37], combined with our results, simultaneously targeting pyroptosis pathways and checkpoint therapy may benefit glioma patients in the high-risk group.

Drugs targeted to the risk lncRNAs and six common chemotherapy drug sensitivities in our signature were also found. For example, in this study, we found that drug sensitivities of fulvestrant, SR16157, and raloxifene were correlated to the expression of TMEM254-AS1. Estrogen receptor fulvestrant as a nonselective antagonist could inhibit medulloblastoma cell growth and migration via restrained ERK1/2 activation [38, 39]. Attwod et al. found that raloxifene controlled and promoted cell death during hypoxia by preventing stress granule dissolution, which impaired translational function [40]. In addition, elevated expression of LINC01088 was associated with drug resistance of imexon, ABT-199, cyclophosphamide, hydroxyurea, chelerythrine, and fostamatinib. Cyclophosphamide was usually used for autoimmune disease therapy, recently study executed by Du and Waxman found that cyclophosphamide may contribute antitumor efficacy at medium dose intermittent which induces ICD and releases type I interferon in GL261 and CT-2A glioma cells [41]. Hydroxyures was a key organic compound for cancer therapy in the management of malignant melanoma, and head and neck cancers [42], a phase I clinical trial of PTK787 plus imatinib and hydroxyurea was applied in glioma patients, it showed that the strategy was safe for recurrent glioma patients [43]. Chelerythrine was a useful chemotherapeutic drug for GBM via inhibiting the TGFB1-ERK1/2/Smad2/3-Snail/ZEB1 signaling pathway. Reversely, higher expression of LINC00665 indicated glioma cells were more sensitive to cobimetinib. It was confirmed that cobimetinib combined with vemurafenib could overcome resistance to vemurafenib for BRAF-mutant ganglioglioma [44]. It provided several potential drugs for glioma therapy and analyzed their relationship to expression levels and drug sensitivities; detection of the signature lncRNAs expression levels before drug treatment may help guide individualized treatment. Furthermore, we compared six regular chemotherapy drugs including gefitinib cisplatin, cyclopamine, etoposide, sunitinib, and vinlastine in the high- and low-risk groups, and it showed that except for gefitinib. The IC50 of cisplatin, cyclopamine, etoposide, sunitinib, and vinlastine were greater in the low-risk group. In short, these outcomes highlighted that our selected lncRNAs and signature may provide drug guidance for glioma patients to improve their outcomes.

To verify the reliability of our model genes, the relationship between COX10-AS1 and pyroptosis was verified by U87 glioma cells in vitro, and it has been confirmed that COX10-AS1 was an oncogenic role involved in cell proliferation and invasion of glioma cells via affecting tumor cell growth by CXO10-AS1/miR-641/E2F6 feedback loop [18] and COX10-AS1/miR-361-5p/ACTG1 [19], but no studies have tested its correlation with pyroptosis. In the current research, it was found that the COX10-AS1 expression was higher in U87 cells than in HMC3 cells. shRNA was conducted to specifically reduce the COX10-AS1 expression level in U87 cells, similar result of proliferation assay was demonstrated in this study, the proliferation ability of cells in the sh-COX10-AS1 group was inhibited. Furthermore, we found that the levels of IL-1β, IL-18, CASP1, and NLRP3 expression were increased after knockdown of COX10-AS1, which indicated that reducing COX10-AS1 might impede tumor progress via inducing glioma cell pyroptosis, and it was a potential therapeutic strategy for glioma, but more detailed tests were needed to carry out.

There were some limitations in our study. First, despite a large number of glioma patients, our data was mainly retrieved from public databases. The present study was short of prospective clinical data verification, so it is necessary to collect patient samples and RNA-sequencing data to establish our verification cohort. In addition, though we applied shRNA to knock down COX10-AS1 in our study, the precise mechanism of model lncRNAs regulated pyroptosis was still unknown; it should be elucidated by further studies in vivo and in vitro.

To sum up, we developed a pyroptosis-related lncRNA signature that exhibited potent ability and accuracy for predicting OS in patients with glioma; it was strongly associated with the immune landscape in the glioma microenvironment, and it provided potential targeted drugs and guidance for individual chemotherapy.

Data Availability

The cohort datasets collected and evaluated in our research can be accessed online on the Cancer Genome Atlas (TCGA) (https://portal.gdc.cancer.gov/) and the Chinese Glioma Genome Atlas (CGGA) (http://www.cgga.org.cn/).

Conflicts of Interest

The study's authors confirmed that there were no financial or commercial connections that may be viewed as having a potential conflict of interest.

Authors' Contributions

Xiaoqiang Feng carried out bioinformatic analyses and wrote the paper. Yuehua Chen, Xuanyu Liu, and Zhihui Zhong performed partially in vitro experiments. Yanjun Liu designed and organized the study. The final manuscript was reviewed and approved by all authors.

Acknowledgments

Supplementary Materials

Supplementary 1. Pyroptosis-related genes Supplementary Table 1. Top ten hub genes analyzed by cytoHubba. Supplementary Table 2. Correlation of potential drugs and risk lncRNAs Supplementary Table 3.

Supplementary 2. Supplementary Figure S1. GO and KEGG pathways involved in the pyroptosis-related lncRNA signature of the TCGA cohort. (A) GO annotation. (B) KEGG pathways.

Supplementary 3. Supplementary Figure S2. The difference of TMB between the high- and low-risk groups. (A) Correlation of TMB scores and risk scores. (B) The difference of TMB scores between the high- and low-risk groups. (C, D) The top 20 genes with the highest mutation frequencies.

References

[1] F. B. Furnari, T. Fenton, R. M. Bachoo et al., "Malignant astrocytic glioma: genetics, biology, and paths to treatment," *Genes & Development*, vol. 21, no. 21, pp. 2683–2710, 2007.

[2] S. Lapointe, A. Perry, and N. A. Butowski, "Primary brain tumours in adults," *The Lancet*, vol. 392, no. 10145, pp. 432–446, 2018.

[3] P. Wesseling and D. Capper, "WHO 2016 classification of gliomas," *Neuropathology and Applied Neurobiology*, vol. 44, no. 2, pp. 139–150, 2018.

[4] W. Wick, M. Weller, M. Van Den Bent et al., "*MGMT* testing—the challenges for biomarker-based glioma treatment," *Nature Reviews. Neurology*, vol. 10, no. 7, pp. 372–385, 2014.

[5] H. Yan, D. W. Parsons, G. Jin et al., "IDH1 and IDH2 mutations in gliomas," *The New England Journal of Medicine*, vol. 360, no. 8, pp. 765–773, 2009.

[6] P. Yu, X. Zhang, N. Liu, L. Tang, C. Peng, and X. Chen, "Pyroptosis: mechanisms and diseases," *Signal Transduction and Targeted Therapy*, vol. 6, no. 1, p. 128, 2021.

[7] T. Bergsbaken, S. L. Fink, and B. T. Cookson, "Pyroptosis: host cell death and inflammation," *Nature Reviews. Microbiology*, vol. 7, no. 2, pp. 99–109, 2009.

[8] X. Lu, T. Guo, and X. Zhang, "Pyroptosis in cancer: friend or foe?," *Cancers (Basel).*, vol. 13, no. 14, p. 3620, 2021.

[9] X. Xia, X. Wang, Z. Cheng et al., "The role of pyroptosis in cancer: pro-cancer or pro-"host"?," *Cell Death & Disease*, vol. 10, no. 9, p. 650, 2019.

[10] X. Ma, P. Guo, Y. Qiu et al., "Loss of AIM2 expression promotes hepatocarcinoma progression through activation of mTOR-S6K1 pathway," *Oncotarget*, vol. 7, no. 24, pp. 36185–36197, 2016.

[11] J. Gao, X. Qiu, G. Xi et al., "Downregulation of GSDMD attenuates tumor proliferation via the intrinsic mitochondrial apoptotic pathway and inhibition of EGFR/Akt signaling and predicts a good prognosis in non-small cell lung cancer," *Oncology reports*, vol. 40, no. 4, pp. 1971–1984, 2018.

[12] Z. Peng, C. Liu, and M. Wu, "New insights into long noncoding RNAs and their roles in glioma," *Molecular Cancer*, vol. 17, no. 1, p. 61, 2018.

[13] K. Yoshihara, M. Shahmoradgoli, E. Martínez et al., "Inferring tumour purity and stromal and immune cell admixture from expression data," *Nature Communications*, vol. 4, no. 1, p. 2612, 2013.

[14] A. M. Newman, C. L. Liu, M. R. Green et al., "Robust enumeration of cell subsets from tissue expression profiles," *Nature Methods*, vol. 12, no. 5, pp. 453–457, 2015.

[15] S. Hänzelmann, R. Castelo, and J. Guinney, "GSVA: gene set variation analysis for microarray and RNA-seq data," *BMC Bioinformatics*, vol. 14, p. 7, 2013.

[16] W. C. Reinhold, M. Sunshine, H. Liu et al., "CellMiner: a web-based suite of genomic and pharmacologic tools to explore transcript and drug patterns in the NCI-60 cell line set," *Cancer Research*, vol. 72, no. 14, pp. 3499–3511, 2012.

[17] U. T. Shankavaram, S. Varma, D. Kane et al., "CellMiner: a relational database and query tool for the NCI-60 cancer cell lines," *BMC Genomics*, vol. 10, p. 277, 2009.

[18] L. Liu, X. Li, H. Wu, Y. Tang, X. Li, and Y. Shi, "The COX10-AS1/miR-641/E2F6 feedback loop is involved in the progression of glioma," *Frontiers in Oncology*, vol. 11, article 648152, 2021.

[19] C. Zhou, X. Jiang, A. Liang et al., "COX10-AS1 facilitates cell proliferation and inhibits cell apoptosis in glioblastoma cells at post-transcription level," *Neurochemical Research*, vol. 45, no. 9, pp. 2196–2203, 2020.

[20] M. Kist and D. Vucic, "Cell death pathways: intricate connections and disease implications," *The EMBO Journal*, vol. 40, no. 5, article e106700, 2021.

[21] D. Wu, S. Wang, G. Yu, and X. Chen, "Cell death mediated by the pyroptosis pathway with the aid of nanotechnology: prospects for cancer therapy," *Angewandte Chemie (International Ed. in English)*, vol. 60, no. 15, pp. 8018–8034, 2021.

[22] N. Ren, T. Jiang, C. Wang et al., "LncRNA ADAMTS9-AS2 inhibits gastric cancer (GC) development and sensitizes chemoresistant GC cells to cisplatin by regulating miR-223-3p/NLRP3 axis," *Aging*, vol. 12, no. 11, pp. 11025–11041, 2020.

[23] H. Yan, B. Luo, X. Wu et al., "Cisplatin induces pyroptosis via activation of MEG3/NLRP3/caspase-1/GSDMD pathway in triple-negative breast cancer," *International Journal of Biological Sciences*, vol. 17, no. 10, pp. 2606–2621, 2021.

[24] C. Tan, W. Liu, Z.-H. Zheng, and X.-G. Wan, "LncRNA HOT-TIP inhibits cell pyroptosis by targeting miR-148a-3p/AKT2 axis in ovarian cancer," *Cell Biology International*, vol. 45, no. 7, pp. 1487–1497, 2021.

[25] G. Tanzhu, N. Li, Z. Li, R. Zhou, and L. Shen, "Molecular subtypes and prognostic signature of pyroptosis-related lncRNAs in glioma patients," *Frontiers in Oncology*, vol. 12, article 779168, 2022.

[26] Z. Xing, Z. Liu, X. Fu et al., "Clinical significance and immune landscape of a pyroptosis-derived LncRNA signature for glioblastoma," *Frontiers in Cell and Development Biology*, vol. 10, article 805291, 2022.

[27] P. Han, J.-W. Li, B.-M. Zhang et al., "The lncRNA CRNDE promotes colorectal cancer cell proliferation and chemoresistance via miR-181a-5p-mediated regulation of Wnt/β-catenin signaling," *Molecular Cancer*, vol. 16, no. 1, p. 9, 2017.

[28] F. Zhang, H. Wang, J. Yu et al., "LncRNA CRNDE attenuates chemoresistance in gastric cancer via SRSF6-regulated

alternative splicing of PICALM," *Molecular Cancer*, vol. 20, no. 1, p. 6, 2021.

[29] D. Fu, L. Zang, Z. Li, C. Fan, H. Jiang, and T. Men, "Long noncoding RNA CRNDE regulates the growth and migration of prostate cancer cells by targeting microRNA-146a-5p," *Bioengineered*, vol. 12, no. 1, pp. 2469–2479, 2021.

[30] J. Zheng, X. Liu, P. Wang et al., "Retracted: CRNDE promotes malignant progression of glioma by attenuating miR-384/PIWIL4/STAT3 Axis," *Molecular Therapy*, vol. 24, no. 7, pp. 1199–1215, 2016.

[31] Z. Zhao, M. Liu, W. Long et al., "Knockdown lncRNA CRNDE enhances temozolomide chemosensitivity by regulating autophagy in glioblastoma," *Cancer Cell International*, vol. 21, no. 1, p. 456, 2021.

[32] J. Zheng, Z. Zhou, Y. Qiu et al., "A prognostic ferroptosis-related lncRNAs signature associated with immune landscape and radiotherapy response in glioma," *Frontiers in Cell and Development Biology*, vol. 9, article 675555, 2021.

[33] S. Nyström, D. J. Antoine, P. Lundbäck et al., "TLR activation regulates damage-associated molecular pattern isoforms released during pyroptosis," *The EMBO Journal*, vol. 32, no. 1, pp. 86–99, 2013.

[34] K. Tsuchiya, S. Nakajima, S. Hosojima et al., "Caspase-1 initiates apoptosis in the absence of gasdermin D," *Nature Communications*, vol. 10, no. 1, article 2091, 2019.

[35] Q. Wang, R. Imamura, K. Motani, H. Kushiyama, S. Nagata, and T. Suda, "Pyroptotic cells externalize eat-me and release find-me signals and are efficiently engulfed by macrophages," *International Immunology*, vol. 25, no. 6, pp. 363–372, 2013.

[36] J. Lu, W. Shi, B. Liang et al., "Efficient engulfment of necroptotic and pyroptotic cells by nonprofessional and professional phagocytes," *Cell Discov.*, vol. 5, no. 1, p. 39, 2019.

[37] J. Hou, R. Zhao, W. Xia et al., "PD-L1-mediated gasdermin C expression switches apoptosis to pyroptosis in cancer cells and facilitates tumour necrosis," *Nature Cell Biology*, vol. 22, no. 10, pp. 1264–1275, 2020.

[38] S. M. Belcher, X. Ma, and H. H. Le, "Blockade of estrogen receptor signaling inhibits growth and migration of medulloblastoma," *Endocrinology*, vol. 150, no. 3, pp. 1112–1121, 2009.

[39] M. Kirby, A. Zsarnovszky, and S. M. Belcher, "Estrogen receptor expression in a human primitive neuroectodermal tumor cell line from the cerebral cortex: estrogen stimulates rapid ERK1/2 activation and receptor-dependent cell migration," *Biochemical and Biophysical Research Communications*, vol. 319, no. 3, pp. 753–758, 2004.

[40] K. M. Attwood, A. Robichaud, L. P. Westhaver et al., "Raloxifene prevents stress granule dissolution, impairs translational control and promotes cell death during hypoxia in glioblastoma cells," *Cell Death & Disease*, vol. 11, no. 11, p. 989, 2020.

[41] B. Du and D. J. Waxman, "Medium dose intermittent cyclophosphamide induces immunogenic cell death and cancer cell autonomous type I interferon production in glioma models," *Cancer Letters*, vol. 470, pp. 170–180, 2020.

[42] K. Madaan, D. Kaushik, and T. Verma, "Hydroxyurea: a key player in cancer chemotherapy," *Expert Review of Anticancer Therapy*, vol. 12, no. 1, pp. 19–29, 2012.

[43] D. A. Reardon, M. J. Egorin, A. Desjardins et al., "Phase I pharmacokinetic study of the vascular endothelial growth factor receptor tyrosine kinase inhibitor vatalanib (PTK787) plus imatinib and hydroxyurea for malignant glioma," *Cancer*, vol. 115, no. 10, pp. 2188–2198, 2009.

[44] M. Touat, J. Gratieux, S. Condette Auliac et al., "Vemurafenib and cobimetinib overcome resistance to vemurafenib inBRAF-mutant ganglioglioma," *Neurology*, vol. 91, no. 11, pp. 523–525, 2018.